Title: Meioc-Piwil1 complexes regulate rRNA transcription for differentiation of spermatogonial stem cells

Toshihiro Kawasaki[1,2]*, Toshiya Nishimura[3], Naoki Tani[4], Carina Ramos[5] Emil Karaulanov[6], Minori Shinya[1,2], Kenji Saito[1], Emily Taylor[5], Rene F. Ketting[6], Kei-ichiro Ishiguro[4], Minoru Tanaka[3], Kellee R. Siegfried[5], Noriyoshi Sakai[1,2]*

[1]Department of Gene Function and Phenomics, National Institute of Genetics, and [2]Department of Genetics, School of Life Science, SOKENDAI (The Graduate University for Advanced Studies), Mishima 411-8540, Japan.

[3]Division of Biological Science, Nagoya University, Nagoya 464-8601, Japan

[4]Institute of Molecular Embryology and Genetics, Kumamoto University, Kumamoto 860-0811, Japan

[5] Biology Department, University of Massachusetts Boston, Boston, MA 02125

[6]Institute of Molecular Biology (IMB), 55128 Mainz, Germany

*Corresponding author

Toshihiro Kawasaki, tokawasa@nig.ac.jp; Noriyoshi Sakai, nosakai@nig.ac.jp

Abstract

Ribosome biogenesis is vital for sustaining stem cell properties, yet its regulatory mechanisms are obscure. Herein, we show unique properties of zebrafish *meioc* mutants in which spermatogonial stem cells (SSCs) do not differentiate or upregulate rRNAs. Meioc colocalized with Piwil1 in perinuclear germ granules, but Meioc depletion resulted in Piwil1 accumulation in nucleoli. Nucleolar Piwil1 interacted with 45S pre-rRNA. *piwil1*$^{+/-}$ spermatogonia with reduced Piwil1 upregulated rRNAs, and *piwil1*$^{+/-}$;*meioc*$^{-/-}$ spermatogonia recovered differentiation later than those in *meioc*$^{-/-}$. Further, Piwil1 interacted with Setdb1 and HP1α, and *meioc*$^{-/-}$ spermatogonia exhibited high levels of H3K9me3 and methylated CpG in the 45S-rDNA region. These results indicate that zebrafish SSCs silence rRNA transcription with repressive marks similar to *Drosophila* piRNA targets of RNA polymerase II, and that Meioc has a unique function on preventing localization of Piwil1 in nucleoli to upregulate rRNA transcripts and to promote SSC differentiation.

Introduction

The maintenance and control of the differentiation of adult stem cells are indispensable for living animals. In this decade, the relationship between the stem cell system and translation activity control has been revealed. Compared with that of differentiating progenitor cells, the global translation activity is generally inhibited in most adult and embryonic stem (ES) cells, and low translation activity is required for stem cells to maintain undifferentiated status (Ni and Buszczak, 2023; Saba et al., 2021). Despite this common feature of low translational activity, differences in the state of ribosome biogenesis (RiBi) have been observed across stem cell types. ES cells, hair follicle stem cells and *Drosophila* germline stem cells (GSCs) are characterized by high levels of RiBi, whereas quiescent neural stem cells (NSCs) express low levels of ribosomal genes **(**Llorens-Bobadilla et al., 2015**)**. Hematopoietic stem cells (HSCs) have higher RiBi levels than differentiated bone marrow cells, but they have lower levels than their immediate progenitors, suggesting that cell type-specific mechanisms may regulate RiBi (Jarzebowski et al., 2018). In addition, phenotypes of ribosome biogenesis defects in *Drosophila* GSCs appear to be controversial; attenuation of Pol I activity and the U3 snoRNP complex member *wiched* (*wcd*) mutant show premature differentiation (Fichelson et al., 2009; Zhang et al., 2014), while knockdown of ribosome assembly and loss of DExD/H-box proteins that govern RiBi result in a loss of differentiation (Martin et al., 2022; Sanchez et al., 2016). Therefore, the mechanisms by which RiBi is coupled to proper stem cell differentiation are still obscure.

By using an ENU mutagenesis screen to identify gonadogenesis defects in zebrafish (Saito et al., 2011), we isolated a unique mutant, *minamoto* (*moto*), in which germ cells arrest at

the early stage of spermatogonia (Kawasaki et al., 2016). By whole genome sequencing, we found that the *moto* phenotype is tightly linked to a mutation within a gene (ENSDARG00000090664) (Bowen et al., 2012), which encodes the coiled-coil domain-containing protein Meioc. Database analysis shows orthologs of MEIOC in vertebrates and most invertebrates, but not in *Drosophila*. The mouse MEIOC has a function to maintain an extended meiotic prophase I with its binding partner YTHDC2 (Abby et al., 2016; Soh et al., 2017). On the other hand, a complex of *Drosophila bam* (*bag of marbles*), a functional homolog of *Meioc*, and *bgcn* (*benign gonial cell neoplasm*), a paralog of *Ythdc2* (Jain et al., 2018), plays a pivotal role in promoting stem cell differentiation (Perinthottathil and Kim, 2011). Although zebrafish *meioc* (*moto*) is an orthologous to the mice gene, it appears to be functionally similar to *Drosophila bam*, making it interesting to see how it controls the development of germ cells.

The present study revealed that zebrafish had spermatogonial stem cells (SSCs) with low rRNA transcription, a characteristic that differed from many other stem cells, and that Meioc was required for upregulation of rRNA transcription and SSC differentiation. Independently of Ythdc2, Meioc regulated intracellular localization of Piwil1 that interacted with transcriptional silencing proteins, Setdb1 (Eggless) and HP1α (Cbx5). Our results suggested that rRNA silencing maintained the undifferentiated state of zebrafish SSCs, providing a new insight on the relationship between the stem cell system and the RiBi control.

Results

Failure to differentiate spermatogonia in the zebrafish *meioc* mutant

In fish testes, germ cells are surrounded by Sertoli cells within a basement membrane compartment and develop synchronously in cysts. Thus, the developmental stage of spermatogonia can be determined by the number of cells within the cyst (**Figure 1A**). Wild-type spermatogonial cells undergo 8 rounds of cell division before entering meiosis (Leal et al., 2009), however *moto*^{t31533} mutant testes had only up to 3 rounds of division, containing 2-8 spermatogonia per cyst (**Figure 1B**). Mutant spermatogonia were positive for the undifferentiated spermatogonia marker, Plzf, which is expressed in single- to 8-cell (1-8-cell) cyst spermatogonia in the wildtype (**Figure 1B**) (Ozaki et al., 2011), but negative for meiotic markers, Sycp1 and Sycp3 (Saito et al., 2014, 2011). Phosphohistone H3 immunostaining indicated that mutant spermatogonia proliferated, but apoptotic cells were increased in the mutant spermatogonia (**Figure S1A**). In zebrafish, mutants that fail to undergo oocyte development become male sex type (Saito et al., 2011; Houwing et al., 2007; Kamminga et al., 2010; Rodríguez-Marí et al., 2010; Shive et al., 2010). Similarly, no females developed in *moto* mutants (**Supplemental Table S1** and **Figure S1B**), as completion of initial stages of meiosis I are a pre-requisite for follicle formation (Elkouby and Mullins, 2017). These results suggested that the *moto*^{t31533} mutant germ cells remained in an undifferentiated state.

By whole genome sequencing and genetic analysis, we found that the *moto*^{t31533} mutant phenotype was tightly linked to a mutation within the ortholog of mouse *meioc* gene (**Figure S1C**) (Bowen et al., 2012). The *moto*^{t31533} mutant inherited the phenotypes described above for more than 10 generation. Furthermore, fish homozygous for another allele, *moto*^{sa13122}, exhibited the same gonadal phenotype as *moto*^{t31533} homozygotes, and *moto*^{sa13122} failed to complement *moto*^{t31533} confirming that these mutations disrupt the same gene (hereafter denoted *meioc*^{mo})

(**Figure S1D**). We searched for paralogues of *meioc* gene using the conserved coiled-coil domain (PF15189) (**Figure S1C**) but were not able to find another gene in GRCz11 (version 111.11). We then generated an antibody against the N-terminus of Meioc (**Figures S1E** and **F**) and could not detect the expression of truncated Meioc in the mutants (**Figure S1G**).

Zebrafish *meioc* RNA and protein signals were observed in a portion of 1-2-cell cyst germ cells in juvenile gonads at 25 days post-fertilization (dpf), adult ovaries and testes (**Figure S2A**). The cells exhibited a large nucleolus, characteristics of presumed germline stem cells (GSCs) in zebrafish (Kawasaki et al., 2016) and stem-type self-renewing type I germ cells in medaka (Nishimura et al., 2015). Both clear RNA and protein signals were detected in premeiotic germ cell clusters, and the protein was detected as granular structures in the cytoplasm with increasing sizes among cells until meiotic prophase I (**Figures S2A-C**).

Upregulation of translation is required for the differentiation of spermatogonia

Since the global translation activity is generally inhibited in stem cells, we analyzed global translational activities of zebrafish spermatogonia using the O-propargyl-puromycin (OP-Puro) assay (Liu et al., 2012). In wildtype, we observed low levels of de novo protein synthesis in a portion of 1-2-cell cyst spermatogonia and high levels in almost all large cysts with more than 32 cells (32≤-cell) of differentiated spermatogonia (**Figures 1C** and **D**). *meioc*$^{mo/mo}$ spermatogonia showed low levels as that of 1-2-cell cysts (**Figures 1C** and **D**). These results suggested that some germ cells within 1-2 cell cysts had low translation activity and that *meioc*$^{mo/mo}$ spermatogonia had low translation activity.

In order to know if translational upregulation is required for differentiation of spermatogonia, we examined the effect of cycloheximide on the development of spermatogonia in vitro. Cycloheximide decreased OP-Puro fluorescence intensities in differentiating spermatogonia with a dose-dependent manner in testis organ culture (**Figure S2D**). At 1.0 μM cycloheximide that reduced OP-Puro fluorescence to approximately 60%, BrdU incorporation decreased in 32≤-cell cysts of spermatogonia, while it was not affected in 1-4-cell spermatogonia (**Figure S2E**). We then examined the effect on differentiation of SSCs using a culture system, in which differentiation can be induced on the Sertoli cell line, ZtA6-12 (Kawasaki et al., 2016). After propagation of SSCs for 1 month, we transferred the cells onto ZtA6-12 and treated with lower concentration of cycloheximide at 0.2 μM, which reduced OP-Puro fluorescence to approximately 70%. The treatment maintained SSCs with a large nucleolus and not expressing Sycp3 (**Figures 1E** and **F**). Bmp2 secretion of ZtA6-12 cells was not affected at 0.2 μM cycloheximide (**Figure S2F**), suggesting that the effect on Sertoli cell function was presumed to be minimized. These results suggested that a certain level of translational activity was required for the differentiation of zebrafish SSCs.

meioc mutants do not upregulate rRNAs in 1-2-cell cyst spermatogonia

To estimate the state of ribosome biogenesis, we examined the expression patterns of rRNAs and the ribosomal protein Rpl15 in zebrafish spermatogonia development. Interestingly, the signal intensities of 5.8S, 18S, 28S rRNAs, and Rpl15 were low in a portion of wildtype 1-2-cell cyst spermatogonia (**Figure 2A**). We did not observe a low intensity of 5S rRNA. Those with low signals increased in almost all 32≤-cell cysts and declined in spermatocytes. To

distinguish between cytoplasmic and nucleolar signals, we performed fluorescence *in situ* hybridization of 28S rRNA. We found 1-2 cell cysts with low cytoplasmic signals also had low nucleolar signals (**Figures 2B-D**). Although cytoplasmic 28S rRNA signals increased to 32≤-cell cysts, the highest nucleolar signals were detected in portion of 1-2-cell cysts and declined at 32≤-cell cysts. These results suggest that 1-2 cell cysts contain populations with low and high rRNA transcriptional activity.

We next tested how rRNA levels were affected in *meioc*$^{mo/mo}$ and found low signals of rRNAs and Rpl15 in spermatogonia (**Figure 2A**). We confirmed these data by performing RT-qPCR from isolated spermatogonia using the *sox17::egfp* SSC marker (Kawasaki et al., 2016), reductions in 5.8S, 18S, 28S rRNAs in *meioc*$^{mo/mo}$ were seen (**Figure 2E**). Furthermore, the homolog of *Drosophila* non-LTR retrotransposable element R2 that transposes exclusively into 28S rDNA(Kojima and Fujiwara, 2003) also decreased in *meioc*$^{mo/mo}$. We next analyzed unprocessed 45S pre-rRNA and pre-rRNA intermediates by Northern blot to compare levels between *meioc*$^{mo/mo}$ and the wildtype. Each was normalized to 7SL RNA. In *meioc*$^{mo/mo}$ the amount of 45S and intermediates was reduced, however levels of pre-RNA intermediate to 45S pre-rRNA was similar to wildtype: 0.69 (0.49/0.71, mutant/wildtype) of unprocessed 45S pre-rRNA and 0.61 (0.72/1.19) of pre-rRNA intermediates with the 5' external transcribed spacer (ETS) probe, and 0.33 (0.05/0.15) and 0.35 (0.17/0.48) with the internal transcribed spacer 1 (ITS1) probe (**Figure S3A**). These results indicate that 45S pre-rRNA transcripts were reduced in *meioc*$^{mo/mo}$ yet processing into pre-RNA intermediates was not affected.

Meioc is required for demethylation of CpG in the IGS of 45S rDNA

Features of silenced rDNA loci, DNA methylation, methylation of histone H3K9, and association of HP1α, are known (Grummt, 2007). In eukaryotes, the transcription of each rDNA locus is regulated by DNA methylation and histone modifications in promoter and enhancer regions in the intergenic spacer (IGS) region (Santoro, 2005). Therefore, we examined DNA methylation state in the region. Since the regulatory sequence of rDNA was not identified in teleosts, we identified tandem repeats of 90, 120 and 318 bp in the IGS region of 45S-S rDNA (Locati et al., 2017) (**Figure S3B**), similar to carp (Vera et al., 2003). Unmethylated CpG in the tandem repeats was frequently found in isolated wildtype *sox17::egfp* spermatogonia, while was rare in *meioc*$^{mo/mo}$ (**Figure 2F**). These results suggested that Meioc is needed for demethylation of CpG in the tandem repeats of 45S rDNA IGS region.

meioc and _ythdc2_ mutants exhibit different phenotypes in the early stage of spermatogonia

The RNA helicase YTHDC2 is a binding partner of the MEIOC in mammals (Abby et al., 2016; Soh et al., 2017). Zebrafish spermatogenic cells expressed Ythdc2 (**Figures S4A** and **B**), and pull-down analysis showed zebrafish Meioc interacted with Ythdc2 (**Figure S4C**). It has been recently reported that *ythdc2* KO zebrafish lack germ cells (Li et al., 2022), but staining or expression analysis was not done to confirm that germ cells were completely absent. We separately generated *ythdc2* KO zebrafish by the CRISPR-Cas9 system (**Figure S4A**), and observed that it had up to 8-cell cyst spermatogonia (**Figure 3A**). We observed that the number of 4-8-cell cysts was clearly different between *meioc*$^{mo/mo}$ and *ythdc2*$^{-/-}$; the ratio of 4-8-cell cysts/1-2-cell cysts in the *ythdc2*$^{-/-}$ was almost the same as that in the wildtype, while that in *meioc*$^{mo/mo}$ significantly decreased (**Figures 3B-D**). Furthermore, *ythdc2*$^{-/-}$ spermatogonia

contained both low and high levels of cells with 5.8S, 18S, 28S rRNAs, and Rpl15, similar to the wildtype (**Figure 3E**). The intensity of the 28S rRNA signals in *ythdc2*$^{-/-}$ were almost same as that in the wildtype (**Figure S4D**). These results suggested that Meioc functioned independently of Ythdc2 on the differentiation of 1-2-cell cysts into 4-8-cell cysts.

Meioc interacts with Piwil1 and affects its intracellular localization

To explore partners of Meioc on regulation of rRNA transcription, we performed LC/MS/MS for the Meioc-immunoprecipitate (IP) of SSC-enriched hyperplastic testes (Kawasaki et al., 2016). The results showed the enrichment of germ granule (nuage) components, compared with normal testis (Supplemental Tables S2 and S3). By immunostaining, Meioc colocalized with the germ granule components, Tdrd1 (Huang et al., 2011), Tdrd6a (Roovers et al., 2018), Piwil1 (Houwing et al., 2007), Piwil2 (Houwing et al., 2008), and Ddx4 (Houwing et al., 2007) in wildtype (**Figures S5A** and **B**). In *meioc*$^{mo/mo}$, Piwil1 was strongly detected in the nucleolus, whereas others exhibited the perinuclear localization characteristic of Ddx4-positive granules as in the wildtype (**Figure 4A**). In contrast, we were able to detect low levels of Piwil1 in nucleoli of wildtype 1-4-cell spermatogonia with overexposed detection after the co-staining of the nucleolar marker Fibrillarin (**Figure 4B**). The signals of Piwil1 in Ddx4-positive granules were decreased in *meioc*$^{mo/mo}$ spermatogonia, compared with wildtype (**Figure 4C**). We confirmed that Meioc and PiwilI directly interacted by Co-IP and revealed that Meioc bound Piwil1 through the Coiled coil domain (**Figure 4D**; **Figure S5C**). These results demonstrated that Piwil1 has a property to localize in nucleoli and that Meioc interacts with Piwil1 in perinuclear

germ granules. In addition, we did not detect the accumulation of Piwil1 in nucleoli in *ythdc2*$^{-/-}$ (**Figure S4E**).

Since Piwil1 abnormally accumulated in nucleoli in *meioc*$^{mo/mo}$, we asked whether Piwil1-dependent piRNA generation (Houwing et al., 2007) was affected. The abundance of piRNA production in *meioc*$^{mo/mo}$ testes was detected at similar levels to those of the wildtype (**Figure S5D**). piRNAs derived from 28S, 18S rRNAs and R2 apparently decreased in *meioc*$^{mo/mo}$ probably due to the low expression of rRNA (**Figures S5E-G**). It is unlikely that Meioc critically affected piRNA generation.

A reduction of Piwil1 upregulates rRNA transcripts and recovers the *meioc* mutant phenotype

From the above analysis, it is hypothesized that accumulation of Piwil1 in the nucleolus suppresses rRNA transcription in the *meioc*$^{mo/mo}$ background. Therefore, we examined the rRNA transcript levels and the phenotype of *meioc*$^{mo/mo}$*;piwil*$^{+/-}$ since the *piwil1*$^{-/-}$ depletes germ cells completely before testis differentiation (Houwing et al., 2007). A reduction in Piwil1 was detected in *piwil*$^{+/-}$ testes by Western blot analysis and in the spermatogonia nucleoli by fluorescent immunohistochemistry (**Figures S6A** and **B**). The upregulation of 28S rRNA was observed in the cytoplasm and nucleoli of *piwil1*$^{+/-}$ 1-2-cell spermatogonia as compared to wildtype and *meioc*$^{mo/mo}$*;piwil1*$^{+/-}$ spermatogonia as compared to *meioc*$^{mo/mo}$ (**Figures 5A** and **B**). Consistent with the increased expression of 28S rRNA, we observed the differentiation of *meioc*$^{mo/mo}$*;piwil1*$^{+/-}$ spermatogonia to the 32-cell stage compared to that of *meioc*$^{mo/mo}$, in which spermatogonia rarely develop to the 8-cell stage (**Figures 5C** and **D**). Furthermore, the number

of 4-8-cell cysts increased in *meioc*$^{mo/mo}$;*piwil1*$^{+/-}$ (**Figures 5E** and **F**). The ratio of 4-8-cell to 1-2-cell cysts in *meioc*$^{mo/mo}$;*piwil1*$^{+/-}$ increased compared to that in *meioc*$^{mo/mo}$, and reached at almost the same level as that in wildtype (**Figure 5G**). These results demonstrated that reduction of Piwil1 compensated the suppression of rRNA transcription and the SSC differentiation defect of the *meioc*$^{mo/mo}$ phenotypes.

Piwil1 interacts with nascent 45S pre-rRNA in nucleoli of SSCs

To investigate if nucleolar Piwil1 interact with 45S pre-rRNA, we examined pre-rRNA in the RNA IP (RIP) of Piwil1 by qRT-PCR. Pre-rRNA was associated with Piwil1 compared with the control IgG in the wildtype testis, and was more enriched in *meioc*$^{mo/mo}$ (**Figure 6A**). Furthermore, we examined the effect of actinomycin D (RNA polymerase I (Pol I) and Pol II inhibitor), BMH-21 (Pol I inhibitor) (Colis et al., 2014), and α-amanitin (Pol II inhibitor)(Bensaude, 2011) on nucleolar localization of Piwil1 in the *meioc*$^{mo/mo}$ testis organ culture. The nucleolar signals of Piwil1 declined upon treatment with actinomycin D and BMH-21 but not α-amanitin, suggesting that the pre-rRNA transcript was involved in Piwil1 localization to the nucleolus (**Figure 6B**). Together, these results suggested that Piwil1 interacted with nascent pre-rRNA transcripts in nucleoli of SSCs.

Nucleolar Piwil1 causes accumulation of H3K9me3 and HP1α

Drosophila Piwi requires histone methyltransferase Setdb1 to lead to H3K9me3 deposition, HP1α accumulation, and heterochromatin formation for silencing of Pol II mediated transcription (Jia et al., 2022). We examined if Setdb1 and HP1α are localized in nucleoli using

anti-Setdb1 (**Figure S6C**) and anti-HP1α (**Figures S6D** and **E**) antibodies. Setdb1 was detected in nucleoli in spermatogonia of 1-2-cell cysts in both wildtype and *meioc*$^{mo/mo}$, and co-IP using *meioc*$^{mo/mo}$ testis lysate showed interaction between Piwil1 and Setdb1 (**Figures 6C** and **D**). The higher signal intensity of Setdb1 nucleolar signal was detected in *meioc*$^{mo/mo}$ spermatogonia (**Figure 6E**). To test whether the amount of nucleolar Piwil1 correlates with the silencing state of rDNA loci, we conducted chromatin IP of histone H3K9me3 and Piwil1. Higher interactions of H3K9me3 and Piwil1 with rDNA were detected in *meioc*$^{mo/mo}$ testes, which have increased levels of nucleolar Piwil1, than those in the wildtype (**Figures 6F** and **G**). In addition, lower interactions were detected in *piwil1*$^{+/-}$ testes, which have a low amount of nucleolar Piwil1 (**Figures 6F** and **G**). Furthermore, HP1α was detected in nucleoli in spermatogonia of 1-2-cell cysts in wildtype and *meioc*$^{mo/mo}$, and co-IP using testis lysate and pull-down assay showed interaction between Piwil1 and HP1α (**Figures 6H** and **I**; **Figure S6F**). HP1α was predominantly localized in nucleoli in wildtype and was more accumulated in *meioc*$^{mo/mo}$ (**Figure 6J**). These results indicated that Piwil1 potentially interacted with Setdb1 in nucleoli and led to H3K9me3 formation and HP1α accumulation in rDNA loci in zebrafish spermatogonia.

Meioc expression is correlated with the upregulation of 28S rRNA

To further investigate the relationship with Meioc and upregulation of rRNA in SSCs, we compared the expression patterns of Meioc and 28S rRNA in isolated *sox17::egfp* spermatogonia. Meioc expression ranged from barely detectable to more than 50 granular dots (**Figures 7A**). Nuclear localization of Meioc was observed in some *sox17::egfp* spermatogonia,

while in other spermatogonia and spermatocytes Meioc was detected exclusively in the cytoplasm (Figure S2C, S7A). The 28S rRNA intensity correlated with increasing Meioc granules (**Figures 7A)**. On the other hand, Piwil1 remained expressed at almost the same across most cells (**Figures 7B**). Since nucleoli were difficult to observe in the isolated cells probably due to the isolation procedure for several hours, it was difficult to verify whether Piwil1 was present in the nucleolus when Meioc expression was low. Therefore, we also examined the expression of Piwil1 in 1-2-cell spermatogonia in wildtype testis sections. Piwil1 was detected at almost same levels in all cells as same as the isolated cells (**Figure S7B**). The large nucleolus was observed in the cells with more than 11-50 Meioc granules, and nucleolar localization of Piwil1 was observed in the cells with 11-50 Meioc granules similar to *meioc*$^{mo/mo}$ spermatogonia, but not in the cells with 51≤ Meioc granules. These results support the idea that Meioc inhibits localization of Piwil1 in nucleoli and that Meioc functioned on upregulation of rRNA transcripts by preventing localization of Piwil1 in nucleoli.

Discussion

This study showed that zebrafish had SSCs with low rRNA transcription activity, and that increased activity correlated with differentiation. The state of low rRNA transcription activity is not similar to high RiBi of ES cells or *Drosophila* GSCs, but is closer to the low expression of ribosomal gene of quiescent NSCs (Llorens-Bobadilla et al., 2015). Since zebrafish SSCs has long term BrdU-retaining germ cells in undifferentiated spermatogonia (Nóbrega et al., 2010), low RiBi may be one of the mechanisms in quiescent cells, although HSCs show high RiBi. Zebrafish 1-2-cell cyst spermatogonia had low and high nucleolar 28S rRNA subpopulations,

and the high rRNA cells were not found in *meioc* mutants. Therefore, high rRNA is considered to be an activated state for differentiation. The progenitor 32≤-cell cysts had highest translational activity and lower rRNA transcriptional activity than high 1-2-cell cysts.

Our results also revealed that Meioc was required for the reduction of H3K9me3 levels and demethylation of CpG at rDNA loci. As shown in Figure 7C, Meioc prevented nucleolar localization of Piwil1. Piwil1 interacted with Setdb1 and both proteins could be found in the nucleolus. Furthermore, high levels of H3K9me3 and HP1α correlated with higher levels of nucleolar Piwil1. This is similar to *Drosophila* Piwi in piRNA-dependent gene silencing for Pol II transcribed genes (Jia et al., 2022). These data support the model that nucleolar Piwil1 interacts with Setdb1 in the nucleolus to silence rDNA transcription via H3K9me3 and recruiting HP1α while Meioc promotes differentiation by blocking Piwil1 nucleolar localization and allowing rDNA transcription. The epigenetic state of tandem repeats of the zebrafish rDNA IGS region was similar to human silenced rDNA with CpG hypermethylation, levels of H3K9me3, and HP1α association (Grummt, 2007). The tandem repeats have been reported as enhancers of rRNA in *Xenopus* (Pikaard and Reeder, 1988), and the methylation status of the region is accompanied by rRNA synthesis (Bird et al., 1981). Since Setdb1 associates with Tip5, which is known to interact with DNA methyltransferase as a component of nucleolar remodeling complex (NoRC)(Yuan et al., 2007; Bersaglieri and Santoro, 2019), the Setdb1 that is interacted with nucleolar Piwil1 in this study is presumed to lead to CpG methylation in rDNA IGS region.

The phenotypes of the zebrafish *meioc* mutants and *ythdc2* mutants are different from those of mouse *Meioc* KO and *Ythdc2* KO, which arrest at meiotic prophase I or immature

follicles (Abby et al., 2016; Soh et al., 2017; Wojtas et al., 2017). In addition to different timing of those expression between mice and zebrafish, the amino acid sequence of Meioc between mice and zebrafish is not well conserved (28.5%), while that of Ythdc2 is well conserved (65.5%). It is likely that zebrafish Meioc have different binding partners and regulate different processes of germ cell development from mouse MEIOC, causing the distinct phenotypes between these mutants. Many unique partners of Meioc, such as RNA binding proteins, myosin proteins, Tudor domain proteins, heat shock proteins and Cnot1 were found in the present study.

In this study, we revealed the function of Piwil1 in regulating rRNA transcription. In *Drosophila*, nucleolar localization of Piwi and impairment of its localization by inhibition of RNA pol I in ovarian somatic cells and nurse cells, and accumulation of undifferentiated GSC, delay of GSC proliferation and upregulation of R1, R2 and rRNA transcripts in *piwi* mutants have been reported (Fefelova et al., 2017; Mikhaleva et al., 2019, 2015; Yakushev et al., 2016). In *C. elegans*, the nuclear Argonaute protein NRDE-3 binds to ribosomal siRNAs (risiRNA) and is translocated from the cytoplasm to the nucleolus, in which the risiRNA/NRDE complex associates with pre-RNAs and reduces the level of pre-rRNAs (Zhou et al., 2017b, 2017a; Zhu et al., 2018). Therefore, Argonaute proteins appear to have a conserved function on controlling RiBi. This study showed that zebrafish Piwil1 used the analogous machinery for rRNA transcription as Piwi-dependent silencing Pol II transcription in *Drosophila*. Since Meioc was identified as a component of germ granules, the novel function of Piwil1 will open new insights into the interactions of germ granules and nucleoli to regulate RiBi and SSC differentiation.

Materials and Methods

Zebrafish

The *moto*^{t31533} mutant fish were isolated in the Tubingen line by N-ethyl-N-nitrosourea mutagenesis screening as described (Saito et al., 2011). The *moto*^{sa13122} mutants were isolated by the Zebrafish Mutation Project (Kettleborough et al., 2013) and provided by the Zebrafish International Resource Center (ZIRC), Eugene Oregon. We used *piwil1*^{hu2479} line (Houwing et al., 2007), *India* line, *AB* line, *IM* line (Shinya and Sakai, 2011), *vas::egfp* (Krøvel and Olsen, 2002) and *sox17::egfp* (Mizoguchi et al., 2008) transgenic fish. The use of these animals for experimental purposes was approved by the committee on laboratory animal care and use at the National Institute of Genetics (approval identification numbers, 27-12 and 28-13) and the University of Massachusetts Boston Institutional Animal Care and Use Committee (protocol #20120032), and carried out according to the Animal Research Reporting of In Vivo Experiments (ARRIVE) guidelines and to relevant guidelines and regulations.

Identification of the meioc gene

We used whole genome sequencing (WGS) to map the *moto*^{t31533} mutation to an approximately 19 Mb (~14 cM) region on chromosome 3 (Bowen et al., 2012), revealing two nonsynonymous changes within this region. Analysis of the WGS data revealed two nonsynonymous changes within this region. One was a missense mutation affecting the *smg1* gene (ENSDARG00000054570) and the other was a nonsense mutation affecting ENSDARG00000090664, orthologue of human C3H17orf104, now called *Meioc* (Abby et al. 2016). By further recombination mapping of the *moto*^{t31533} mutation using Simple Sequence Length Polymorphisms (SSLPs), the mutation was found in a region of about 2.1 Mb, between

markers z22516 and z8680, which contained the C3H17orf104 locus and excluded the *smg1* locus.

The ythdc2 mutant

The *ythdc2*$^{-/-}$ fish were generated by CRISPR-Cas9 mutagenesis based on protocols (Chen et al., 2017; Hwang et al., 2013). A single-guide RNA (Supplemental Table S5) was designed to target exon 5 of *ythdc2* (ENSDART00000166268.2) to delete functional domains predicted by Pfam 35.0 (Figure S2 F; Mistry et al., 2021)). *ythdc2* sgRNA (100ng/µl) and 10 pmol/µl Cas9 NLS protein (abm) were co-injected into 1-cell stage *India* embryos. Founders were backcrossed with *India* fish, and the F1 siblings were screened by genotyping. Heterozygous *ythdc2* knockout carrying a -14 bp frameshift mutation in exon 5 (*ythdc2*$^{-}$, a -14 bp deletion affecting the codons from G206 that generates 63 amino acid residues from the wrong frame and stop codon after the 269th amino acid) were obtained.

Meioc and Ythdc2 antibodies

To produce specific antibodies against Meioc and Ythdc2, *meioc* cDNA encoding 356 amino acid residues from N-terminus and *ythdc2* cDNA encoding amino acid residue Arg743 to Leu1381 were cloned into a pQE-30 vector (QIAGEN) and a pET-21a (+) vector (Novagen), respectively. The 6 x histidine tag fused proteins were expressed and purified as described previously (Ozaki et al., 2011). Rats and rabbits were immunized with the purified Meioc and Ythdc2 recombinant proteins, respectively. Then, anti-Meioc rat IgG and anti-Ythdc2 rabbit

IgG were purified with CNBr activated sepharose (Cytiva) conjugated with recombinant proteins according to manufacturer's instructions.

Western blot analysis

Western blot analyses were performed as described (Ozaki et al., 2011) using antibodies (Supplemental Table S6). Chemiluminescent signals generated with ECL Prime (GE Healthcare) were detected and quantified with Chemidoc XRS Plus (Bio-Rad). For the quantification of Piwil1, eight wildtype testes and nine *piwil1*$^{+/-}$ testes were individually used for the protein extraction and western blotting analysis. The amount of Piwil1, BMP-2, and α-Tubulin were quantified using quantity tools of ImageLab software version 6.0.1 (Bio-Rad), and Piwil1 and BMP-2 signal intensities were normalized with signal intensities of α-Tubulin.

Histological observation

Testes and juveniles were fixed in 4% PFA in PBS or Bouin's solution (Sigma) for 2 hours at RT. Paraffin sections were prepared at a 5μm thickness and stained with hematoxylin and eosin. For the count of spermatogonial cysts, complete serial sections of 3 testes each of wildtype, *ythdc2*$^{-/-}$, *meioc*$^{mo/mo}$; *piwil1*$^{+/+}$, and *meioc*$^{mo/mo}$; *piwil1*$^{+/-}$ were stained with PAS (periodic acid Schiff) to stain the Sertoli cells (Saito et al., 2014). The number of spermatogonia in cysts were identified by observation of adjacent sections. For wildtype testes, we counted them in randomly selected 10 sections. Undifferentiated spermatogonia (1- to 8-cell spermatogonia) in *ythdc2*$^{-/-}$, *meioc*$^{mo/mo}$; *piwil1*$^{+/+}$, and *meioc*$^{mo/mo}$; *piwil1*$^{+/-}$ testes were counted in randomly selected 10 fields (23547.2 μm^2/ field) of sections, and estimated average number of each stage

of spermatogonia. The area of the sections of wildtype testes and the fields used for the counting were calculated by using ImageJ/Fiji software (Schindelin et al., 2012).

Immunohistochemistry and in situ hybridization in testis sections

Immunohistochemistry was performed with slight modifications as described (Kawasaki et al., 2016). Rehydrated sections were antigen retrieved using Immunosaver reagent (Nisshin EM) as manufacturer's instructions, and blocked with EzBlockChemi (Atto) containing 5% BSA (Sigma). Used antibodies and reagents were listed in supplemental Table S6. To analyze Ddx4, Piwil1, Piwil2, Tdrd1 and Tdrd6 localization in *meioc*$^{mo/mo}$ spermatogonia, we used anti-Ddx4 IgG labeled with fluorescein using Fluorescein labeling kit – NH2 (Dojindo) and performed double staining with other antibodies because all antibodies were generated in rabbits.

In situ hybridization of rRNAs was performed with slight modifications as described (Ozaki et al., 2011). To synthesize digoxingenin (DIG) labeled cRNA probes, cDNA of rRNAs were amplified from RT-PCR of testicular RNA using primer sets (Supplemental Table S5), and cloned into the pGEM-T Easy vector (Promega). Twelve loci of precursor 45S rRNA were identified in zebrafish genome (Locati et al., 2017), we designed the specific primer sets that are able to detect rRNAs derived from more than 6 loci. The DIG labeled cRNA probes were synthesized using DIG RNA labeling kit (Roche). The reagents and antibodies were listed in supplemental Table S6.

For the fluorescence detection, images were obtained under a FV1000 confocal microscope (Olympus). Overexposed Piwil1 images were acquired under conditions of high detector sensitivity ignoring halation of Piwil1 signals in cytoplasm. The signal strength were

quantified using ImageJ/Fiji software (Schindelin et al., 2012). Three testes of wildtype, *meioc*$^{mo/mo}$, *piwil1*$^{+/-}$ and *piwil1*$^{+/-}$ were used for the quantification. The signal intensities were normalized to the intensities of neighboring sperm or the intensities of myoid cells of basement membrane of lobules.

TdT-mediated nick-end labeling (TUNEL)

TUNEL assays were performed using in situ cell death detection kit (AP; Roche, Germany) as described by the manufacturers. The experiments were repeated three times.

Whole-mount in situ hybridization and immunohistochemistry

Whole-mount in situ hybridization and immunohistochemistry were performed as described (Nakamura et al., 2006). A cDNA clone for *meioc* was isolated from RT-PCR of testicular RNA using the primer set (Supplemental Table S5). The digoxingenin (DIG)-labeled RNA probes were synthesized using the *meioc* cDNA and DIG RNA-labeing kit (Roche), and the reagents and antibodies were listed in supplemental Table S6.

Protein synthesis assay

Measurement of protein synthesis of germ cells was performed by the Click-iT Plus OPP Alexa Fluor 594 protein synthesis assay kit (Molecular Probes) with slight modifications as described (Sanchez et al., 2016). The fragments of the *meioc*$^{mo/mo}$ and wildtype *sox17:egfp* testes were treated with Leibovitz's L-15 medium (Sigma) containing a 1:400 dilution of Click-iT OPP reagent at 28 °C for 30 minutes. Fluorescence images were acquired with confocal microscope

(FV-1000, Olympus). Quantification of OP-Puro fluorescence intensity was performed using ImageJ as described (Sanchez et al., 2016). The signal intensities were normalized to the intensities of neighboring sperm and the myoid cells of basement membrane of lobules. The experiments were repeated three times.

Inhibition of ribosome translation in culture

Testis fragments were cultured on the floating membrane in the spermatogonia proliferation medium without growth factors (Kawasaki et al., 2012), with cycloheximide at 0.1 µM, 1.0 µM and 10 µM or the same amount of DMSO as a control for 2 days. Then, BrdU incorporation was analyzed using Cell proliferation kit (GE Healthcare). At least n=3 tissues were examined.

Spermatogonia of a *sox17::egfp* hyperplasia testis were cultured as described (Kawasaki et al., 2016). After 1 month of SSC propagation, SSCs were transferred onto the Sertoli cell line ZtA6-12 to induce differentiation, and 0.2 µM cycloheximide was added. After 9 days, the SSCs (large cells with a few large nucleolus) and the differentiated spermatogonia (small cells with several small nucleolus) were counted according to their morphology and eGFP expression. n=3 dishes were examined.

Co-IP

Co-IP was performed with slight modifications as described (Houwing et al., 2007). Testes were homogenized with cell lysis buffer M (Wako) containing cOmplete,Mini Protease Inhibitor cocktail (Roche). One IP generally contained 20µl protein G beads (Protein G HP SpinTrap,

Cytiva), three testes, and 20µg of antibodies against Meioc or Piwil1 (Supplemental Table S6) in a total volume of 500µl. The experiments were repeated three times.

For RIP, testes were homogenized with 133µl of the lysis buffer containing 100U/ml of SUPERase·In RNase inhibitor (Thermo Fisher Scientific) for 1mg of testis. One IP contains 30µl Dynabeads Protein G (Thermo Fisher Scientific), 7.2 µg of anti-Piwil1 antibody, and 250µl of the lysates. Beads and 1% of the lysates were used for Trizol (Thermo Fisher Scientific) RNA isolation. RNA was reverse transcribed using the PrimeScript RT Reagent Kit with gDNA Eraser (Takara), and used for RT-qPCR with TB Green Premix Ex Taq II (Takara) using LightCycler480 (Roche). The thermal cycling were as follows: initial hold for 2 min at 95 °C followed by 60 cycles of 30 s at 95 °C, 30 s at 58 °C for primer set for unprocessed pre-rRNA (5'ETS-18S rRNA in supplemental Table S5; (Heyn et al., 2017), and 20 s at 72 °C. Fold enrichment was calculated with -ddCt by normalization with input using Sigma RIP-qRT-PCR Data Analysis Calculation Shell, associated with the Sigma Imprint RIP kit (http://www.sigmaaldrich.com/life-science/epigenetics/imprint-rna.html). The experiments were repeated three times.

Mass spectrometry

For mass spectrometry, co-IP using anti-Meioc IgG and Normal rat IgG were performed using normal testes and hypertrophied testes as described above. We used Dynabeads Protein G (Thermo Fisher Scientific) and the anti-Meioc antibody was cross-linked with the beads as described by the manufacturers. The IP was used for Mass spectrometry as described (Ishiguro et al., 2020). The raw LC-MS/MS data was analyzed against the UniProt Knowledgebase

restricted to *Danio rerio* using Proteome Discoverer version 1.4 (Thermo Fisher Scientific) with the Mascot search engine version 2.5 (Matrix Science).

Construction of expression vectors

For transfection of Meioc, Ythdc2, Piwil1, and HP1α, cDNA fragments encoding zebrafish full-length *meioc*, *ythdc2*, *piwil1*, and *hp1α* were amplified by RT-PCR using primer sets (Supplemental Table S5). The amplified fragments of *meioc*, *ythdc2* and *piwil1* were subcloned into a pFLAG-CMV-5a expression vector (Sigma-Aldrich) by using EcoRI and SalI, to create a FLAG tag at the C-terminus of the expressed protein. The amplified fragment was assembled via overlap sequence using NEBuilder HiFi DNA Assembly Master Mix (New England BioLabs). Each 500ng of plasmids were used for transfection to the cells cultured in 35mm dish.

For transfection of *Escherichia coli* (Rosetta-gami2 (Novagen)), cDNA fragments encoding zebrafish *dnmt3Aa*, *dnmt3Ab*, *dnmt3Ba*, *dnmt3Bb1*, *dnmt3Bb2*, *dnmt3Bb3*, and *hp1α* were amplified by RT-PCR using primer sets (Supplemental Table S5), and cloned into the pET-21a (+) vector (Novagen) using NEBuilder HiFi DNA Assembly Mix (New England BioLabs). Expression of cloned cDNAs were induced with 1μM Isopropyl-β-D-thiogalactopyranoside (IPTG, Wako).

Pull-down assay

The expression vectors were transfected into HEK-293 cells using Lipofectamine 3000 Transfection Reagent (Thermo Fisher Scientific). After 48 h, cells were harvested and used for

immunoprecipitation as described above. We used anti-Flag M2 agarose resin (Sigma). The experiments were repeated three times.

Small RNA-seq library preparation and sequencing

Total RNA from 6 *meioc*$^{+/mo}$ and 5 *meioc*$^{mo/mo}$ testis samples at 10 months old was isolated using Trizol RNA isolation according to manufacturer's instructions (Thermo Fisher Scientific). RNAs smaller than 40nt were isolated using a 15% TBE-Urea polyacrylamide gel (BioRad), and purified with sodium chloride/isopropanol precipitation. NGS library preparation was performed using the NEBNext Multiplex Small RNA Library Prep Set for Illumina (New England BioLabs) as recommended by the manufacturer (protocol version v2.0 8/13), with 14 PCR cycles for library amplification. The PCR-amplified DNA was purified using AMPure XP beads (Beckman Coulter). Size selection of the small RNA library was done on LabChip XT instrument (Perkin Elmer) using a DNA 300 assay kit. The library fractions in the range 120-161 bp were pooled in equal molar ratio. The resulting 2nM pool was denatured and diluted to 10 pM with 5% PhiX spike-in DNA and sequenced (single read, 51 cycles, high output mode) on 2 lanes of HiSeq 2000 system (Illumina).

Small RNA-seq data analysis

The raw NGS reads in FastQ format were cleaned from partial 3' adapter sequences using Flexbar v.2.4 (Dodt et al., 2012) using parameters: *-m 18 -ao 10 -as AGATCGGAAGAGCACACGTCTGAACTCCAGTCAC*. Read mapping to the Danio rerio reference genome (Zv9/danRer7 build from Illumina iGenomes) was carried out using Bowtie

v.0.12.8(Langmead et al., 2009) with parameters: *-n 0 -e 80 -l 18 -y --best --nomaqround*. Reads were assigned to the predicted zebrafish 28S and 18S rRNAs, defined as 4110 nt and 1887 nt sequences from GenBank records CT956064 and BX537263 with highest Megablast homology to the respective rRNAs from Cyprinus carpio (GenBank JN628435), as well as to the zebrafish R2 transposon (GenBank AB097126), using Bowtie with perfect match parameters (-v 0 -m 1). Quality assessment of the raw data and length profiling of the mapped reads was performed with FastQC (http://www.bioinformatics.babraham.ac.uk/projects/fastqc). The sequence data have been deposited in the NCBI GEO repository (http://www.ncbi.nlm.nih.gov/geo) under accession number GSE84060. [The temporal token (password) for reviewers access to the GEO record before publication is: wjunoeqmrxidpep]

Inhibition of RNA polymerases

Fragments of *meioc*$^{mo/mo}$ testes were cultured in the spermatogonia proliferation medium without growth factors (Kawasaki et al., 2012). Actinomycin D (Wako) at 1 µg/ml, α-amanitin (Bensaude, 2011) at 10 µg/ml and BMH-21 (Sigma) (Colis et al., 2014) at 1 µM were added. After 1 hr incubation at 28˚ in 5% CO_2/20% O_2, testicular samples were fixed and analyzed by immunohistochemistry for Piwil1. The experiments were repeated three times.

In situ hybridization and immunocytochemistry of isolated spermatogonia

After sorting spermatogonia of *sox17::egfp* wild-type that expresses EGFP at the equivalent stage to *meioc*$^{mo/mo}$ spermatogonia (Kawasaki et al., 2012) using JSAN cell sorter (Bay Bioscience), cells were plated on the CREST-coated glass slides (Matsunami) for 10 minutes,

and fixed with 4% paraformaldehyde for 10 minutes. The cells were treated with 0.5% Triton X100 in PBS for 5 minutes. To detect 28S rRNA, the cells were acetylated with 0.025% acetic anhydrid in triethanolamine 10mM for 5 minutes and followed as described above. After hybridization, antibodies and reagents (Supplemental Table S6) were used. Images were obtained under a FV1000 confocal microscope (Olympus). The signal strength of 28S rRNA, Meioc and Piwil1 was quantified using ImageJ/Fiji software (Schindelin et al., 2012). The signal intensities of in situ hybridization (28S rRNA) and immunocytochemistry (Meioc and Piwil1) were normalized to the intensities of S probe and control IgG, respectively.

DNA methylation analysis

Because there was no information of the structure of IGS region in zebrafish, we analyzed IGS sequence of known active locus of 45S-S rDNA (Ch5: 831,755-826,807 in GRCz11) (Locati et al., 2017) using Tandem repeats finder software (Benson, 1999). The result was summarized in the schema of Supplemental Figure S3B. The undifferentiated spermatogonia of *meioc*$^{mo/mo}$*;sox17::egfp* and *sox17::egfp* wildtype were sorted using JSAN cell sorter (Bay Bioscience) and used for bisulfite conversion using MethylEasy Xceed Rapid DNA Bisulfite modification kit (Takara). The tandem repeat region of 45S-S rDNA IGS was amplified by PCR with EpiTaq HS (Takara) using the primer sets (Supplemental Table S5). The primers were designed using Meth primer software (Li and Dahiya, 2002). All PCR products were subcloned into the pCRII vector (Thermo Fisher Scientific) and used for sequencing analysis using online QUMA software (Kumaki et al., 2008).

Comparison of RNA expression levels

After sorting spermatogonia of *vas::egfp; meioc*$^{mo/mo}$ and *sox17::egfp* wildtype that expresses EGFP at the equivalent stage to *meioc*$^{mo/mo}$ spermatogonia using JSAN cell sorter (Bay Bioscience), total RNA were extracted and used for RT-qPCR analysis as described in "Immunoprecipitation" section using primer sets (Supplemental Table S5). Relative gene expression levels were calculated using the comparative Ct method (Schmittgen and Livak, 2008) and normalized to the expression of *gapdh*. The experiments were repeated three times.

Northern blot analysis

Northern blot analysis was performed using DIG northern starter kit (Roche). cDNA fragments of 5'ETS and ITS1 region of 45S-S rDNA(Locati et al., 2017) and 7SL were amplified from RT-PCR of testicular RNA using the primers containing T7 and T3 promoter sequence (Supplemental Table S5) and used for cRNA probe synthesis with T3 RNA polymerase using DIG RNA labeling kit (Roche). Signals of 45S pre-rRNA, pre-rRNA intermediates and 7SL were detected with a Chemidoc XRS Plus (Bio-Rad), and quantified using quantity tools of ImageLab software version 6.0.1 (Bio-Rad). For the quantification, three wildtype and *meioc*$^{mo/mo}$ testes were individually used. Signal intensities of 45S pre-rRNA, pre-rRNA intermediates were normalized with signal intensities of 7SL.

Chromatin IP (ChIP)-qPCR analysis

Chip assay was performed with slight modifications as described (Imai et al., 2017). Ten testes were used for 6 ml of chromatin suspension. Sonication was carried out with a Bioruptor®

Standard apparatus (Diagenode) at high power for four series of 7 cycles (30 s on, 30 s off). For IP, 1 ml of chromatin suspension was incubated with 20 µl of Dynabeads® Protein A (Thermo Fisher Scientific) pre-incubated with 3 µg of rabbit anti-histone H3 tri-methyl K9 (Abcam, ab8898) and Piwil1 antibodies. Quantitative PCR (qPCR) was performed with SYBR Premix Ex Taq II (Takara) using LightCycler480 (Roche) using primer sets (Supplemental Table S5). Fold enrichment was calculated with -ddCt by normalization with 10% input sample using Sigma RIP-qRT-PCR Data Analysis Calculation Shell, associated with the Sigma Imprint RIP kit (http://www.sigmaaldrich.com/life-science/epigenetics/imprint-rna.html). The experiments were repeated six times.

Quantification and Statistical analysis

Data were presented as the mean ± standard deviation of at least three independent experiments as indicated in each method and figure legend. Statistical difference between two groups was determined using unpaired Student's *t*-test when the variance was heterogeneous between the groups, and Welch's *t*-test was used when the variance was heterogeneous. $P < 0.05$ was considered statistically significant. Graphical presentations were made with the R package ggplot2 (Wickham, 2009).

Competing interest statement: The authors declare no competing financial interests.

Acknowledgments

We thank C. Nüsslein-Volhard for supporting the ENU mutagenesis screening and providing the

anti-Ddx4 antibody, K. Saito and Y. Kato for providing advice, Y. Saga for reading the manuscript, Y. Yoshida and Y. Yamazaki for maintaining the zebrafish stocks, and the IMB Genomics and Bioinformatics Core Facilities. Isolation of the *moto* mutant was supported by EC Contract LSHG-CT-2003-503496 and *meioc*^{sa13122} was provided by the Zebrafish International Resource Center. This work was supported by JSPS KAKENHI Grant Numbers JP23116709, JP25251034, JP25114003 to NS, JST A-step Grant Numbers JPMJTR204F to NS, the program of the Inter-University Research Network for High Depth Omics, IMEG, Kumamoto University to NS. C.R. was supported by the UMB Initiative for Maximizing Student Development program, NIH award R25 GM076321.

Author Contributions

Toshihiro Kawasaki, Kellee R. Siegfried and Noriyoshi Sakai conceived and designed the work. Toshihiro Kawasaki, Toshiya Nishimura, Naoki Tani, Carina Ramos, Emil Karaulanov, Minori Shinya, Kenji Saito, Emily Taylor, Rene F. Ketting, Kei-ichiro Ishiguro, Minoru Tanaka, Kellee R. Siegfried and Noriyoshi Sakai performed the experiments and analyzed the data. Toshihiro Kawasaki, Kellee R. Siegfried and Noriyoshi Sakai wrote the manuscript.

References

Abby E, Tourpin S, Ribeiro J, Daniel K, Messiaen S, Moison D, Guerquin J, Gaillard J-C, Armengaud J, Langa F, Toth A, Martini E, Livera G. 2016. Implementation of meiosis prophase I programme requires a conserved retinoid-independent stabilizer of meiotic transcripts. *Nat Commun* **7**:10324. doi:10.1038/ncomms10324

Bensaude O. 2011. Inhibiting eukaryotic transcription. Which compound to choose? How to evaluate its activity?: Which compound to choose? How to evaluate its activity?

Transcription **2**:103–108. doi:10.4161/trns.2.3.16172

Benson G. 1999. Tandem repeats finder: a program to analyze DNA sequences. *Nucleic Acids Res* **27**:573–580. doi:10.1093/nar/27.2.573

Bersaglieri C, Santoro R. 2019. Genome Organization in and around the Nucleolus. *Cells* **8**:579. doi:10.3390/cells8060579

Bird A, Taggart M, Macleod D. 1981. Loss of rDNA methylation accompanies the onset of ribosomal gene activity in early development of X. laevis. *Cell* **26**:381–390. doi:10.1016/0092-8674(81)90207-5

Bowen ME, Henke K, Siegfried KR, Warman ML, Harris MP. 2012. Efficient Mapping and Cloning of Mutations in Zebrafish by Low-Coverage Whole-Genome Sequencing. *Genetics* **190**:1017–1024. doi:10.1534/genetics.111.136069

Chen JS, Dagdas YS, Kleinstiver BP, Welch MM, Sousa AA, Harrington LB, Sternberg SH, Joung JK, Yildiz A, Doudna JA. 2017. Enhanced proofreading governs CRISPR–Cas9 targeting accuracy. *Nature* **550**:407–410. doi:10.1038/nature24268

Colis L, Peltonen K, Sirajuddin P, Liu H, Sanders S, Ernst G, Barrow JC, Laiho M. 2014. DNA intercalator BMH-21 inhibits RNA polymerase I independent of DNA damage response. *Oncotarget* **5**:4361–4369. doi:10.18632/oncotarget.2020

Dodt M, Roehr J, Ahmed R, Dieterich C. 2012. FLEXBAR—Flexible Barcode and Adapter Processing for Next-Generation Sequencing Platforms. *Biology* **1**:895–905. doi:10.3390/biology1030895

Elkouby YM, Mullins MC. 2017. Methods for the analysis of early oogenesis in Zebrafish. *Dev Biol* **430**:310–324. doi:10.1016/j.ydbio.2016.12.014

Fefelova EA, Stolyarenko AD, Yakushev EY, Gvozdev VA, Klenov MS. 2017. Participation of the piRNA pathway in recruiting a component of RNA polymerase I transcription initiation complex to germline cell nucleoli. *Mol Biol* **51**:718–723. doi:10.1134/S0026893317050089

Fichelson P, Moch C, Ivanovitch K, Martin C, Sidor CM, Lepesant J-A, Bellaiche Y, Huynh J-R. 2009. Live-imaging of single stem cells within their niche reveals that a U3snoRNP component segregates asymmetrically and is required for self-renewal in Drosophila. *Nat Cell Biol* **11**:685–693. doi:10.1038/ncb1874

Grummt I. 2007. Different epigenetic layers engage in complex crosstalk to define the epigenetic state of mammalian rRNA genes. *Hum Mol Genet* **16**:R21–R27. doi:10.1093/hmg/ddm020

Heyn P, Salmonowicz H, Rodenfels J, Neugebauer KM. 2017. Activation of transcription enforces the formation of distinct nuclear bodies in zebrafish embryos. *RNA Biol* **14**:752–760. doi:10.1080/15476286.2016.1255397

Houwing S, Berezikov E, Ketting RF. 2008. Zili is required for germ cell differentiation and meiosis in zebrafish. *EMBO J* **27**:2702–2711. doi:10.1038/emboj.2008.204

Houwing S, Kamminga LM, Berezikov E, Cronembold D, Girard A, Van Den Elst H, Filippov DV, Blaser H, Raz E, Moens CB, Plasterk RHA, Hannon GJ, Draper BW, Ketting RF. 2007. A Role for Piwi and piRNAs in Germ Cell Maintenance and Transposon Silencing in Zebrafish. *Cell* **129**:69–82. doi:10.1016/j.cell.2007.03.026

Huang H-Y, Houwing S, Kaaij LJT, Meppelink A, Redl S, Gauci S, Vos H, Draper BW, Moens CB, Burgering BM, Ladurner P, Krijgsveld J, Berezikov E, Ketting RF. 2011. Tdrd1 acts as a molecular scaffold for Piwi proteins and piRNA targets in zebrafish: Tdrd1 as a scaffold for Piwi-pathway activity. *EMBO J* **30**:3298–3308. doi:10.1038/emboj.2011.228

Hwang WY, Fu Y, Reyon D, Maeder ML, Kaini P, Sander JD, Joung JK, Peterson RT, Yeh J-RJ. 2013. Heritable and Precise Zebrafish Genome Editing Using a CRISPR-Cas System. *PLoS ONE* **8**:e68708. doi:10.1371/journal.pone.0068708

Imai Y, Baudat F, Taillepierre M, Stanzione M, Toth A, De Massy B. 2017. The PRDM9 KRAB domain is required for meiosis and involved in protein interactions. *Chromosoma* **126**:681–695. doi:10.1007/s00412-017-0631-z

Ishiguro K, Matsuura K, Tani N, Takeda N, Usuki S, Yamane M, Sugimoto M, Fujimura S, Hosokawa M, Chuma S, Ko MSH, Araki K, Niwa H. 2020. MEIOSIN Directs the Switch from Mitosis to Meiosis in Mammalian Germ Cells. *Dev Cell* **52**:429-445.e10. doi:10.1016/j.devcel.2020.01.010

Jain D, Puno MR, Meydan C, Lailler N, Mason CE, Lima CD, Anderson KV, Keeney S. 2018. ketu mutant mice uncover an essential meiotic function for the ancient RNA helicase YTHDC2. *eLife* **7**:e30919. doi:10.7554/eLife.30919

Jarzebowski L, Le Bouteiller M, Coqueran S, Raveux A, Vandormael-Pournin S, David A, Cumano A, Cohen-Tannoudji M. 2018. Mouse adult hematopoietic stem cells actively synthesize ribosomal RNA. *RNA* **24**:1803–1812. doi:10.1261/rna.067843.118

Jia D-D, Jiang H, Zhang Yi-Fei, Zhang Y, Qian L-L, Zhang Yin-Feng. 2022. The regulatory function of piRNA/PIWI complex in cancer and other human diseases: The role of DNA methylation. *Int J Biol Sci* **18**:3358–3373. doi:10.7150/ijbs.68221

Kamminga LM, Luteijn MJ, Den Broeder MJ, Redl S, Kaaij LJT, Roovers EF, Ladurner P, Berezikov E, Ketting RF. 2010. Hen1 is required for oocyte development and piRNA stability in zebrafish. *EMBO J* **29**:3688–3700. doi:10.1038/emboj.2010.233

Kawasaki T, Saito K, Sakai C, Shinya M, Sakai N. 2012. Production of zebrafish offspring from cultured spermatogonial stem cells. *Genes Cells* **17**:316–325. doi:10.1111/j.1365-2443.2012.01589.x

Kawasaki T, Siegfried KR, Sakai N. 2016. Differentiation of zebrafish spermatogonial stem cells to functional sperm in culture. *Development* dev.129643. doi:10.1242/dev.129643

Kettleborough RNW, Busch-Nentwich EM, Harvey SA, Dooley CM, De Bruijn E, Van Eeden F, Sealy I, White RJ, Herd C, Nijman IJ, Fényes F, Mehroke S, Scahill C, Gibbons R, Wali N, Carruthers S, Hall A, Yen J, Cuppen E, Stemple DL. 2013. A systematic genome-wide analysis of zebrafish protein-coding gene function. *Nature* **496**:494–497. doi:10.1038/nature11992

Kojima KK, Fujiwara H. 2003. Cross-Genome Screening of Novel Sequence-Specific Non-LTR Retrotransposons: Various Multicopy RNA Genes and Microsatellites Are Selected as Targets. *Mol Biol Evol* **21**:207–217. doi:10.1093/molbev/msg235

Krøvel AV, Olsen LC. 2002. Expression of a vas::EGFP transgene in primordial germ cells of the zebrafish. *Mech Dev* **116**:141–150. doi:10.1016/S0925-4773(02)00154-5

Kumaki Y, Oda M, Okano M. 2008. QUMA: quantification tool for methylation analysis. *Nucleic Acids Res* **36**:W170–W175. doi:10.1093/nar/gkn294

Langmead B, Trapnell C, Pop M, Salzberg SL. 2009. Ultrafast and memory-efficient alignment of short DNA sequences to the human genome. *Genome Biol* **10**:R25. doi:10.1186/gb-2009-10-3-r25

Leal MC, Cardoso ER, Nóbrega RH, Batlouni SR, Bogerd J, França LR, Schulz RW. 2009. Histological and Stereological Evaluation of Zebrafish (Danio rerio) Spermatogenesis with an Emphasis on Spermatogonial Generations1. *Biol Reprod* **81**:177–187. doi:10.1095/biolreprod.109.076299

Li L, Krasnykov K, Homolka D, Gos P, Mendel M, Fish RJ, Pandey RR, Pillai RS. 2022. The XRN1-regulated RNA helicase activity of YTHDC2 ensures mouse fertility independently of m6A recognition. *Mol Cell* **82**:1678-1690.e12. doi:10.1016/j.molcel.2022.02.034

Li L-C, Dahiya R. 2002. MethPrimer: designing primers for methylation PCRs.

Bioinformatics **18**:1427–1431. doi:10.1093/bioinformatics/18.11.1427

Liu J, Xu Y, Stoleru D, Salic A. 2012. Imaging protein synthesis in cells and tissues with an alkyne analog of puromycin. *Proc Natl Acad Sci* **109**:413–418. doi:10.1073/pnas.1111561108

Llorens-Bobadilla E, Zhao S, Baser A, Saiz-Castro G, Zwadlo K, Martin-Villalba A. 2015. Single-Cell Transcriptomics Reveals a Population of Dormant Neural Stem Cells that Become Activated upon Brain Injury. *Cell Stem Cell* **17**:329–340. doi:10.1016/j.stem.2015.07.002

Locati MD, Pagano JFB, Girard G, Ensink WA, Van Olst M, Van Leeuwen S, Nehrdich U, Spaink HP, Rauwerda H, Jonker MJ, Dekker RJ, Breit TM. 2017. Expression of distinct maternal and somatic 5.8S, 18S, and 28S rRNA types during zebrafish development. *RNA* **23**:1188–1199. doi:10.1261/rna.061515.117

Martin ET, Blatt P, Nguyen E, Lahr R, Selvam S, Yoon HAM, Pocchiari T, Emtenani S, Siekhaus DE, Berman A, Fuchs G, Rangan P. 2022. A translation control module coordinates germline stem cell differentiation with ribosome biogenesis during Drosophila oogenesis. *Dev Cell* **57**:883-900.e10. doi:10.1016/j.devcel.2022.03.005

Mikhaleva EA, Leinsoo TA, Ishizu H, Gvozdev VA, Klenov MS. 2019. The nucleolar transcriptome regulates Piwi shuttling between the nucleolus and the nucleoplasm. *Chromosome Res* **27**:141–152. doi:10.1007/s10577-018-9595-y

Mikhaleva EA, Yakushev EY, Stolyarenko AD, Klenov MS, Rozovsky YaM, Gvozdev VA. 2015. Piwi protein as a nucleolus visitor in Drosophila melanogaster. *Mol Biol* **49**:161–167. doi:10.1134/S0026893315010100

Mistry J, Chuguransky S, Williams L, Qureshi M, Salazar GA, Sonnhammer ELL, Tosatto SCE, Paladin L, Raj S, Richardson LJ, Finn RD, Bateman A. 2021. Pfam: The protein families database in 2021. *Nucleic Acids Res* **49**:D412–D419. doi:10.1093/nar/gkaa913

Mizoguchi T, Verkade H, Heath JK, Kuroiwa A, Kikuchi Y. 2008. Sdf1/Cxcr4 signaling controls the dorsal migration of endodermal cells during zebrafish gastrulation. *Development* **135**:2521–2529. doi:10.1242/dev.020107

Nakamura S, Kobayashi D, Aoki Y, Yokoi H, Ebe Y, Wittbrodt J, Tanaka M. 2006. Identification and lineage tracing of two populations of somatic gonadal precursors in medaka embryos. *Dev Biol* **295**:678–688. doi:10.1016/j.ydbio.2006.03.052

Ni C, Buszczak M. 2023. Ribosome biogenesis and function in development and

disease. *Development* **150**:dev201187. doi:10.1242/dev.201187

Nishimura T, Sato T, Yamamoto Y, Watakabe I, Ohkawa Y, Suyama M, Kobayashi S, Tanaka M. 2015. *foxl3* is a germ cell–intrinsic factor involved in sperm-egg fate decision in medaka. *Science* **349**:328–331. doi:10.1126/science.aaa2657

Nóbrega RH, Greebe CD, Van De Kant H, Bogerd J, De França LR, Schulz RW. 2010. Spermatogonial Stem Cell Niche and Spermatogonial Stem Cell Transplantation in Zebrafish. *PLoS ONE* **5**:e12808. doi:10.1371/journal.pone.0012808

Ozaki Y, Saito K, Shinya M, Kawasaki T, Sakai N. 2011. Evaluation of Sycp3, Plzf and Cyclin B3 expression and suitability as spermatogonia and spermatocyte markers in zebrafish. *Gene Expr Patterns* **11**:309–315. doi:10.1016/j.gep.2011.03.002

Perinthottathil S, Kim C. 2011. Bam and Bgcn in Drosophila Germline Stem Cell DifferentiationVitamins & Hormones. Elsevier. pp. 399–416. doi:10.1016/B978-0-12-386015-6.00038-X

Pikaard CS, Reeder RH. 1988. Sequence Elements Essential for Function of the *Xenopus laevis* Ribosomal DNA Enhancers. *Mol Cell Biol* **8**:4282–4288. doi:10.1128/mcb.8.10.4282-4288.1988

Rodríguez-Marí A, Cañestro C, BreMiller RA, Nguyen-Johnson A, Asakawa K, Kawakami K, Postlethwait JH. 2010. Sex Reversal in Zebrafish fancl Mutants Is Caused by Tp53-Mediated Germ Cell Apoptosis. *PLoS Genet* **6**:e1001034. doi:10.1371/journal.pgen.1001034

Roovers EF, Kaaij LJT, Redl S, Bronkhorst AW, Wiebrands K, De Jesus Domingues AM, Huang H-Y, Han C-T, Riemer S, Dosch R, Salvenmoser W, Grün D, Butter F, Van Oudenaarden A, Ketting RF. 2018. Tdrd6a Regulates the Aggregation of Buc into Functional Subcellular Compartments that Drive Germ Cell Specification. *Dev Cell* **46**:285-301.e9. doi:10.1016/j.devcel.2018.07.009

Saba JA, Liakath-Ali K, Green R, Watt FM. 2021. Translational control of stem cell function. *Nat Rev Mol Cell Biol* **22**:671–690. doi:10.1038/s41580-021-00386-2

Saito K, Sakai C, Kawasaki T, Sakai N. 2014. Telomere distribution pattern and synapsis initiation during spermatogenesis in zebrafish. *Dev Dyn* **243**:1448–1456. doi:10.1002/dvdy.24166

Saito K, Siegfried KR, Nüsslein-Volhard C, Sakai N. 2011. Isolation and cytogenetic characterization of zebrafish meiotic prophase I mutants. *Dev Dyn* **240**:1779–1792. doi:10.1002/dvdy.22661

Sanchez CG, Teixeira FK, Czech B, Preall JB, Zamparini AL, Seifert JRK, Malone CD, Hannon GJ, Lehmann R. 2016. Regulation of Ribosome Biogenesis and Protein Synthesis Controls Germline Stem Cell Differentiation. *Cell Stem Cell* **18**:276–290. doi:10.1016/j.stem.2015.11.004

Santoro R. 2005. The silence of the ribosomal RNA genes. *Cell Mol Life Sci* **62**:2067–2079. doi:10.1007/s00018-005-5110-7

Schindelin J, Arganda-Carreras I, Frise E, Kaynig V, Longair M, Pietzsch T, Preibisch S, Rueden C, Saalfeld S, Schmid B, Tinevez J-Y, White DJ, Hartenstein V, Eliceiri K, Tomancak P, Cardona A. 2012. Fiji: an open-source platform for biological-image analysis. *Nat Methods* **9**:676–682. doi:10.1038/nmeth.2019

Schmittgen TD, Livak KJ. 2008. Analyzing real-time PCR data by the comparative CT method. *Nat Protoc* **3**:1101–1108. doi:10.1038/nprot.2008.73

Shinya M, Sakai N. 2011. Generation of Highly Homogeneous Strains of Zebrafish Through Full Sib-Pair Mating. *G3 GenesGenomesGenetics* **1**:377–386. doi:10.1534/g3.111.000851

Shive HR, West RR, Embree LJ, Azuma M, Sood R, Liu P, Hickstein DD. 2010. *brca2* in zebrafish ovarian development, spermatogenesis, and tumorigenesis. *Proc Natl Acad Sci* **107**:19350–19355. doi:10.1073/pnas.1011630107

Soh YQS, Mikedis MM, Kojima M, Godfrey AK, De Rooij DG, Page DC. 2017. Meioc maintains an extended meiotic prophase I in mice. *PLOS Genet* **13**:e1006704. doi:10.1371/journal.pgen.1006704

Vera MI, Molina A, Pinto R, Reyes M, Álvarez M, Krauskopf E, Quezada C, Torres J, Krauskopf M. 2003. Genomic organization of the rDNA cistron of the teleost fish Cyprinus carpio. *Biol Res* **36**. doi:10.4067/S0716-97602003000200014

Wickham H. 2009. ggplot2: Elegant Graphics for Data Analysis. New York, NY: Springer New York. doi:10.1007/978-0-387-98141-3

Wojtas MN, Pandey RR, Mendel M, Homolka D, Sachidanandam R, Pillai RS. 2017. Regulation of m6A Transcripts by the 3→5 RNA Helicase YTHDC2 Is Essential for a Successful Meiotic Program in the Mammalian Germline. *Mol Cell* **68**:374-387.e12. doi:10.1016/j.molcel.2017.09.021

Yakushev EY, Mikhaleva EA, Abramov YA, Sokolova OA, Zyrianova IM, Gvozdev VA, Klenov MS. 2016. The role of Piwi nuclear localization in the differentiation and proliferation of germline stem cells. *Mol Biol* **50**:630–637.

doi:10.1134/S0026893316040154

Yuan X, Feng W, Imhof A, Grummt I, Zhou Y. 2007. Activation of RNA Polymerase I Transcription by Cockayne Syndrome Group B Protein and Histone Methyltransferase G9a. *Mol Cell* **27**:585–595. doi:10.1016/j.molcel.2007.06.021

Zhang Q, Shalaby NA, Buszczak M. 2014. Changes in rRNA Transcription Influence Proliferation and Cell Fate Within a Stem Cell Lineage. *Science* **343**:298–301. doi:10.1126/science.1246384

Zhou X, Chen X, Wang Y, Feng X, Guang S. 2017a. A new layer of rRNA regulation by small interference RNAs and the nuclear RNAi pathway. *RNA Biol* **14**:1492–1498. doi:10.1080/15476286.2017.1341034

Zhou X, Feng X, Mao H, Li M, Xu F, Hu K, Guang S. 2017b. RdRP-synthesized antisense ribosomal siRNAs silence pre-rRNA via the nuclear RNAi pathway. *Nat Struct Mol Biol* **24**:258–269. doi:10.1038/nsmb.3376

Zhu C, Yan Q, Weng C, Hou X, Mao H, Liu D, Feng X, Guang S. 2018. Erroneous ribosomal RNAs promote the generation of antisense ribosomal siRNA. *Proc Natl Acad Sci* **115**:10082–10087. doi:10.1073/pnas.1800974115

Figure legends

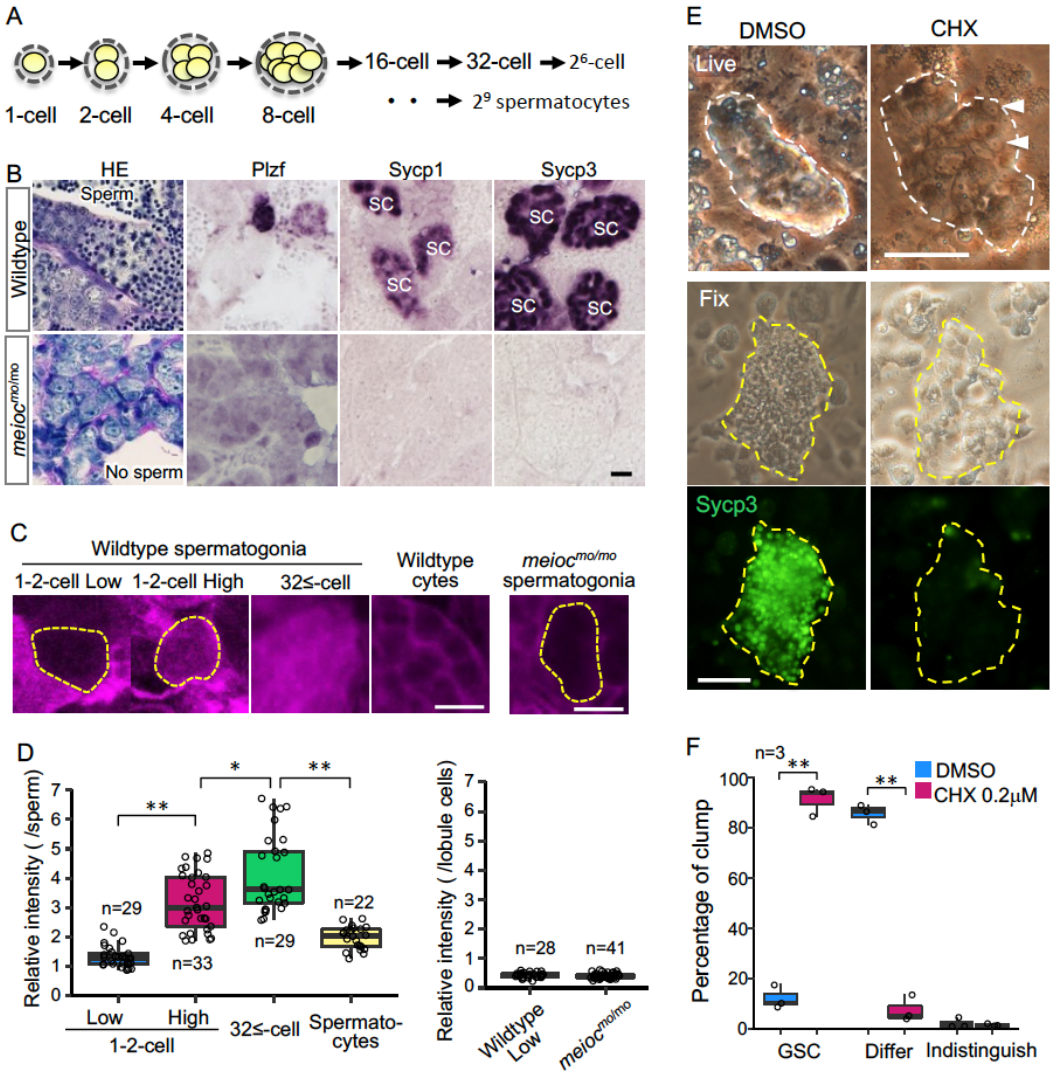

Figure 1. Low translational activity of *meioc* mutant spermatogonia

(A) Schema of the development of spermatogonial cysts surrounded by Sertoli cells in zebrafish. (B) Histology (HE) and immunostaining against Plzf and spermatocyte markers (Sycp1, 3) in the wildtype and the *moto*$^{-/-}$ testes. Scale bar: 10 μm. (C, D) OP-Puro fluorescence analysis (C) and quantification of the signal intensities (D) in wildtype and *meioc*$^{mo/mo}$ spermatogenic cells.

Scale bars: 10 μm. (E-F) Effect of cycloheximide (CHX, 0.2 μM) on differentiation of SSCs in culture. Yellow dotted lines; germ cell clumps. Sycp3; Immunostaining of Sycp3. Arrowheads; examples of a cell with a large nucleolus. The graph (F) presents the percentage of clumps of SSCs and differentiated cells (Differ) shown in Panel E. Scale bar; 50 μm. Data are represented as mean ± SD.

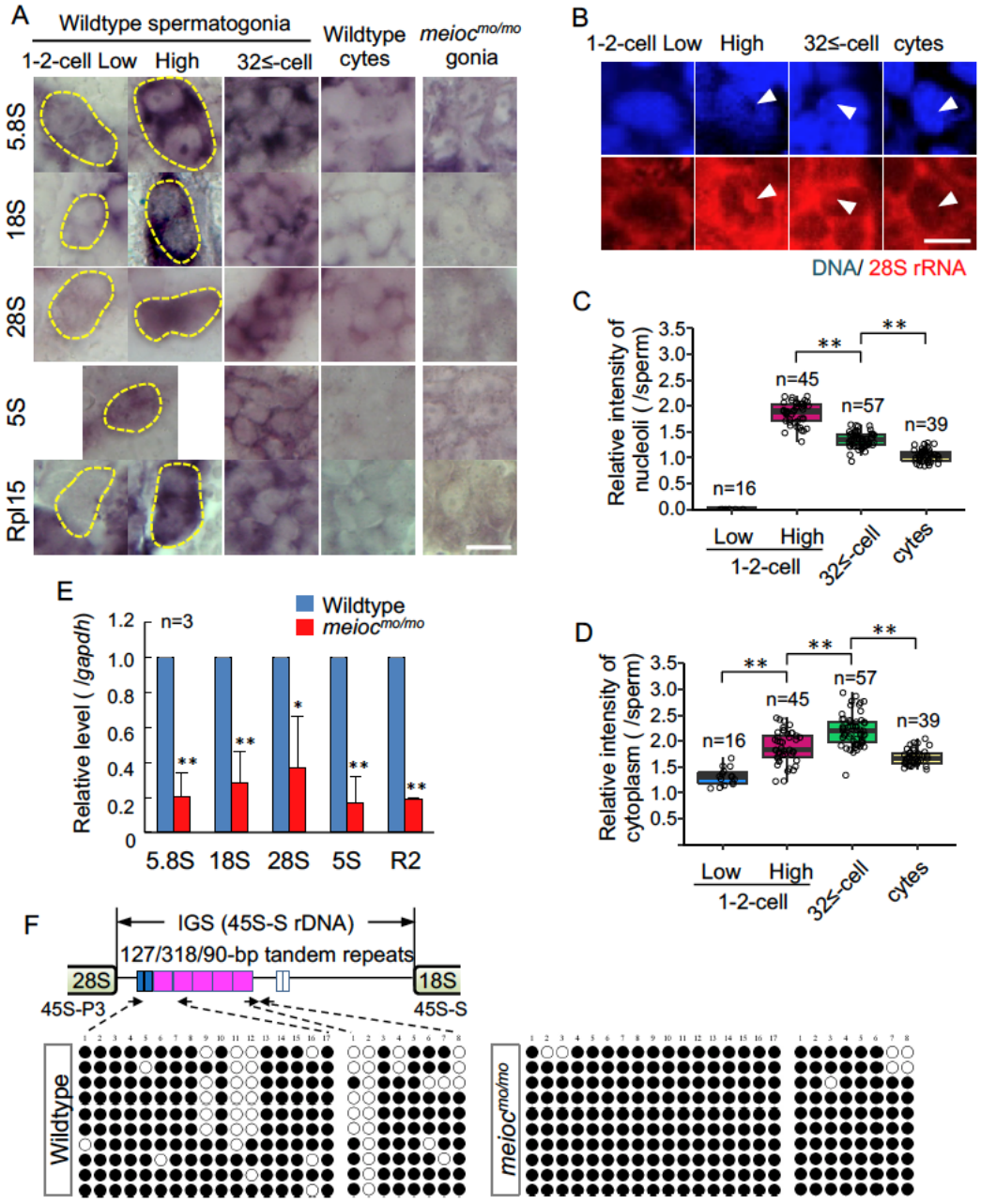

Figure 2. Defect on upregulation of rRNA transcription in *meioc*$^{mo/mo}$ spermatogonia

(A) In situ hybridization of 5S, 5.8S, 18S, and 28S rRNA and immunohistochemistry with anti-Rpl15 antibody in spermatogonia (gonia) and spermatocytes (cyte) in wildtype and *meioc*$^{mo/mo}$. Yellow dotted lines indicate 1-2-cell spermatogonia. (B-D) Fluorescent in situ

hybridization of 28S rRNA in wildtype. The graphs present quantification of signal intensities of 28S rRNA in nucleoli (C) and in cytoplasm (D) in spermatogenic cells. Arrowheads; nucleoli. (E) qRT-PCR analysis of rRNAs and R2 between wildtype and *meioc*$^{mo/mo}$ purified undifferentiated spermatogonia. (F) Bisulfite-sequencing analysis of the tandem repeat region in the IGS region of the 45S-S rDNA locus in purified undifferentiated spermatogonia of wildtype and *meioc*$^{mo/mo}$. Arrows; position of bisulfite primers in the tandem repeat elements (blue, magenta and white boxes), black dots; methylated CpG sites, white dots; unmethylated sites. *p < 0.05, **p < 0.01. Scale bars: 10 µm.

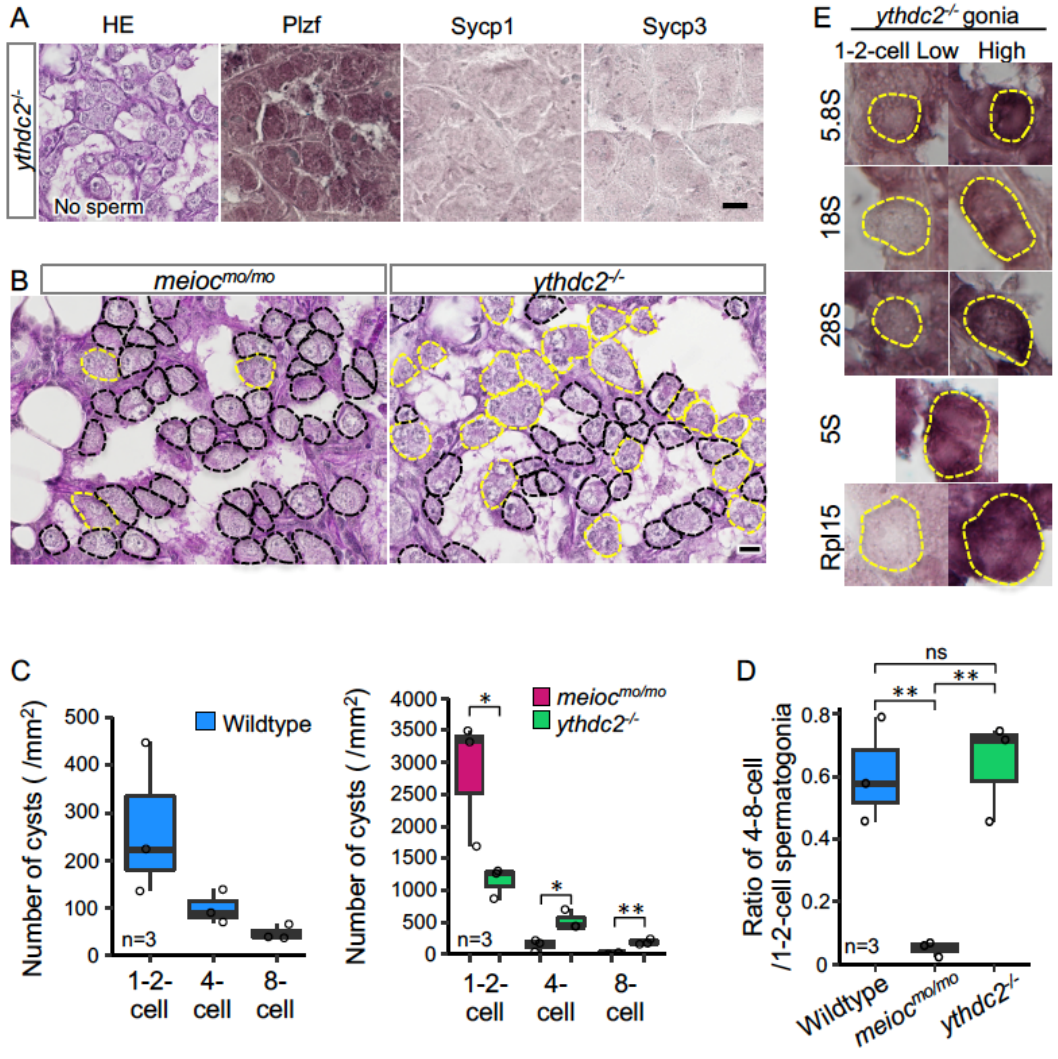

Figure 3. *ythdc2* mutant spermatogonia have different defects from *meioc*$^{mo/mo}$.

(A) Histology (HE) and immunostaining against Plzf and spermatocyte markers (Sycp1, 3) in the *ythdc2*$^{-/-}$ testes. (B) Representative image of *meioc*$^{mo/mo}$ and *ythdc2*$^{-/-}$ testes sections stained with PAS (periodic acid Schiff) and hematoxylin. Dotted lines; 1-2-cell cyst spermatogonia (black) and 4≤-cell cysts (yellow). (C) The number of 1-2-, 4-, and 8-cell cyst spermatogonia per mm^2 of sections in wildtype, *meioc*$^{mo/mo}$ and *ythdc2*$^{-/-}$ testes. (D) Ratio of the number of 4-8-cell cyst spermatogonia to 1-2-cell cysts in wildtype, *meioc*$^{mo/mo}$ and *ythdc2*$^{-/-}$ testes. (E) In

situ hybridization of 5S, 5.8S, 18S, and 28S rRNA and immunohistochemistry with anti-Rpl15 antibody in the *ythdc2*$^{-/-}$ testes. Yellow dotted lines; 1-2-cell spermatogonia. *p < 0.05, **p < 0.01. Scale bars: 10 μm.

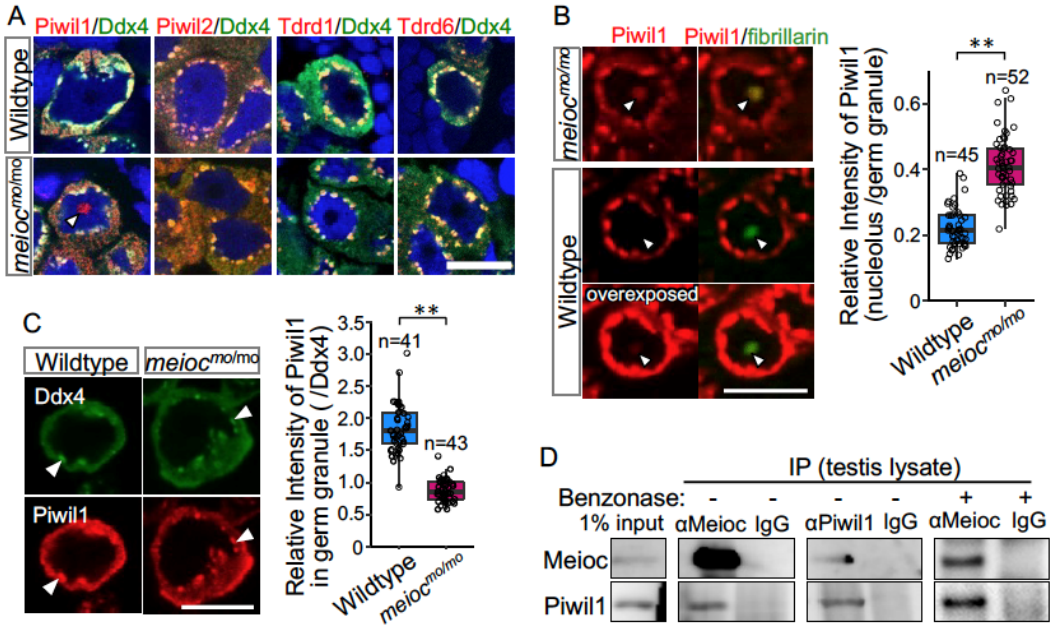

Figure 4. Meioc directly binds with Piwil1 and affects the localization of Piwil1.

(A) Immunostaining of Ddx4 and Piwil1, Piwil2, Tdrd1 and Tdrd6 in wildtype and *meioc*$^{mo/mo}$ spermatogonia. The arrowhead; the Piwil1 signal in the nucleolus. (B) Immunostaining against Piwil1 and fibrillarin (left panels) and quantification of nucleolar Piwil1 (right panel) in wildtype and *meioc*$^{mo/mo}$ spermatogonia. Arrowheads; Fibrillarin positive nucleolus. (C) Immunostaining of Piwil1 and Ddx4 (left panels) and quantification of Piwil1 in germ granules (right panel) in wildtype and *meioc*$^{mo/mo}$ spermatogonia. Arrowheads; Ddx4 positive germ granules. (D) Coimmunoprecipitation of Meioc and Piwil1 using testis lysate. Meioc signals were detected in Piwil1 immunoprecipitate and vice versa. Benzonase: addition of benzonase nuclease. **p < 0.01. Scale bars: 10 µm.

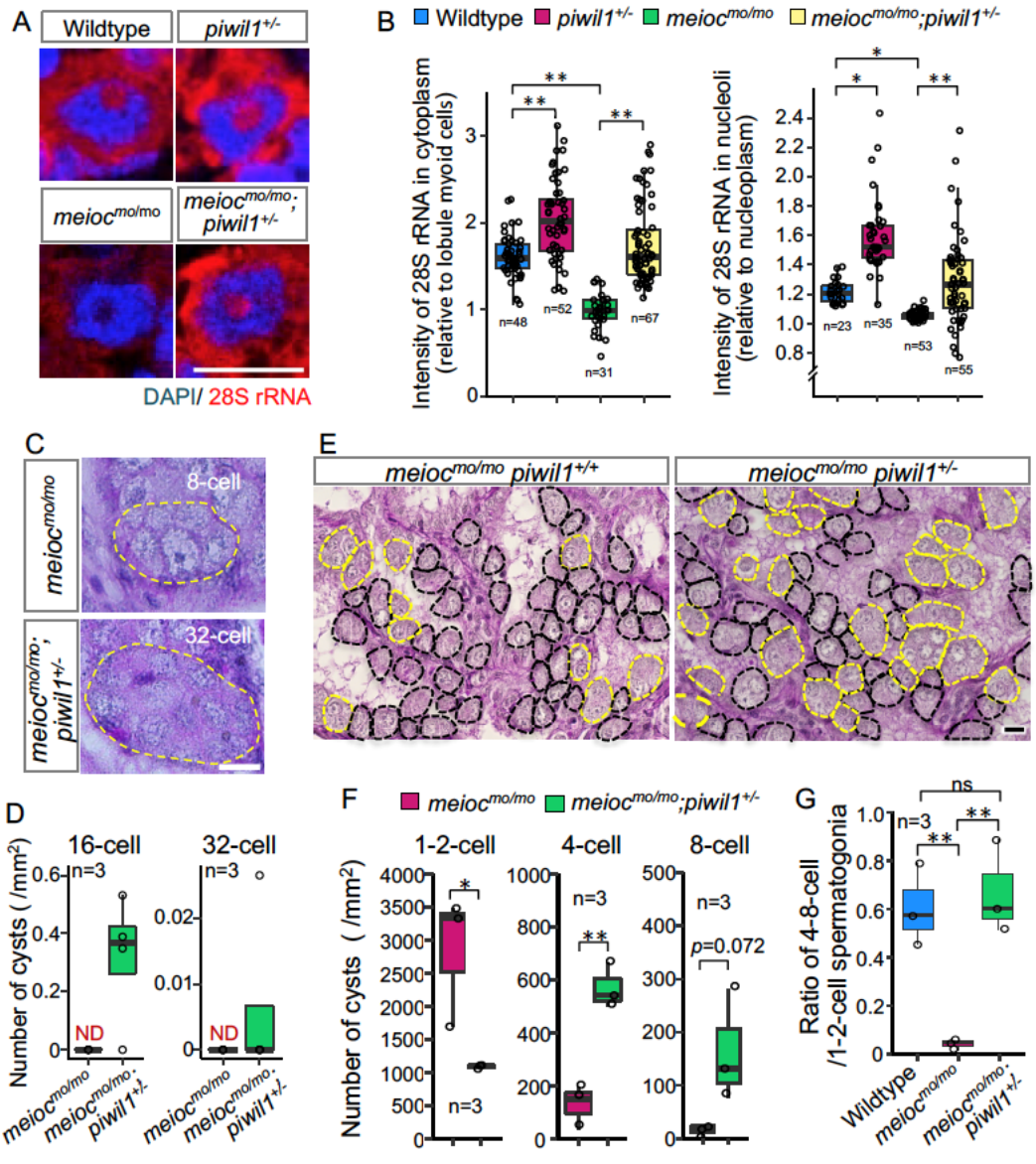

Figure 5. Reduction of Piwil1 compensated phenotypes of *meioc*$^{mo/mo}$.

(A, B) In situ hybridization of 28S rRNA in wildtype and *meioc*$^{mo/mo}$*;piwil1*$^{+/-}$ spermatogonia (1-2-cell cysts). Graphs (B) show the relative signal intensity in the cytoplasm normalized to the intensity of lobule myoid cells (left) and nucleoli normalized to the intensity of the nucleoplasm (right). (C, D) Differentiated spermatogonia in *meioc*$^{mo/mo}$ and *meioc*$^{mo/mo}$*;piwil1*$^{+/-}$testes. Yellow dotted lines; differentiated spermatogonia. Graphs (D) show the number of 16-cell and 32-cell

cyst spermatogonia per mm^2 of sections. ND: not detected. (E-G) *meioc*$^{mo/mo}$ and *meioc*$^{mo/mo}$ *piwil1*$^{+/-}$ testis sections stained with PAS and hematoxylin. Cysts of 1-2-cell spermatogonia (black) and 4≤-cell cysts (yellow) are indicated by dotted lines. Graphs show numbers of 1-, 2-, 4-, and 8-cell cysts per mm^2 in sections of *meioc*$^{mo/mo}$ and *meioc*$^{mo/mo}$*;piwil1*$^{+/-}$ testes (F), and ratio of the number of 4-8-cell cysts to 1-2-cell cysts in wildtype, *meioc*$^{mo/mo}$ and *meioc*$^{mo/mo}$*;piwil1*$^{+/-}$ (G). *$p < 0.05$, **$p < 0.01$. Scale bars: 10 µm.

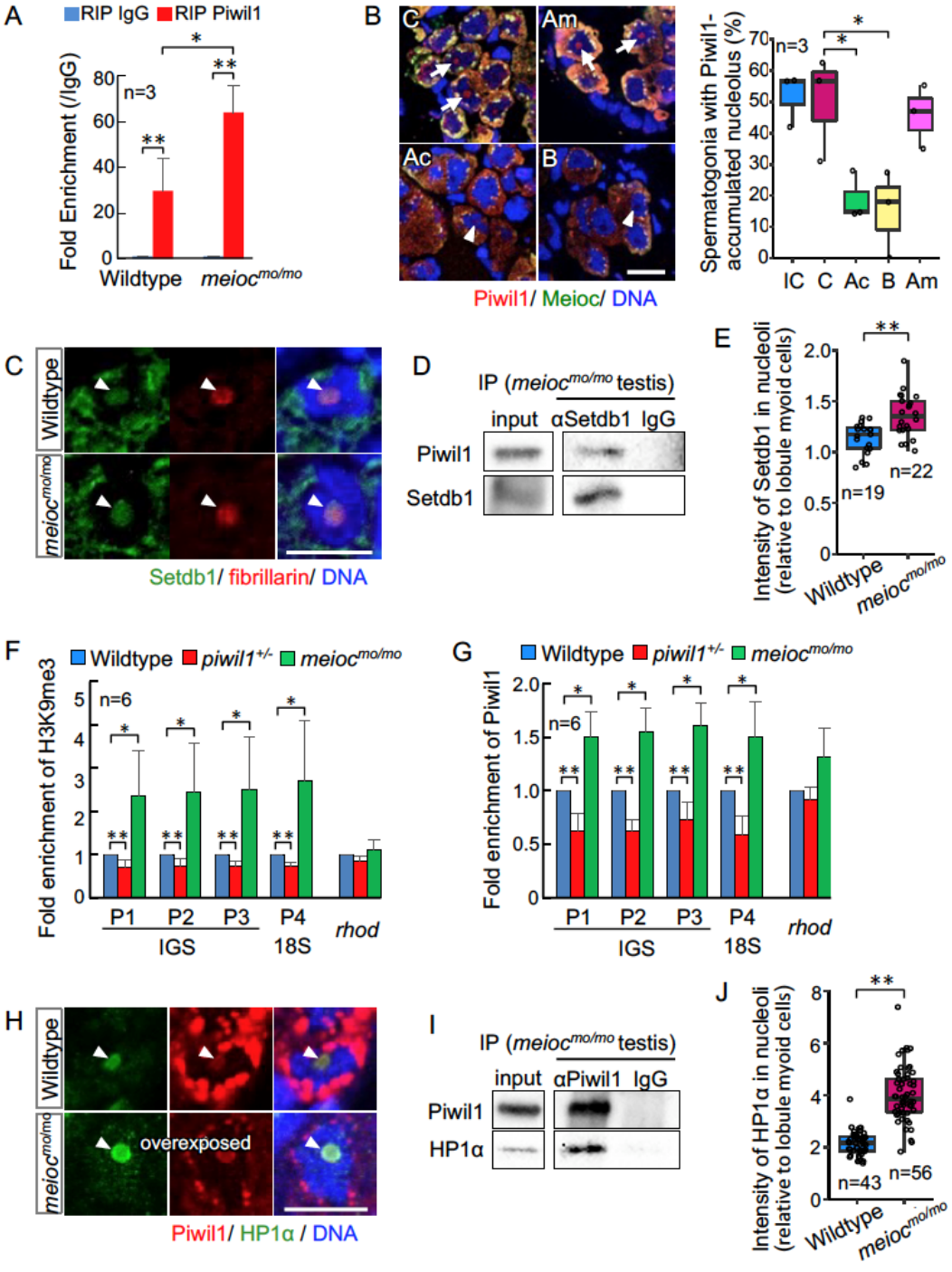

Figure 6. Nucleolar Piwil1 interacted with Setdb1 and causes silenced epigenetic state of rDNA loci

(A) Fold enrichment of pre-rRNA (5'ETS-18S rRNA) in Piwil1 immunoprecipitated RNA relative to the control IgG in wildtype and *meioc*$^{mo/mo}$ testes. (B) Immunostaining of Piwil1 (left panels) and the percentage of spermatogonia with detectable nucleolar Piwil1 (right panel) in the *meioc*$^{mo/mo}$ testes treated with α-amanitin (Am), actinomycin D (Ac) and BMH-21 (B). Arrows; Piwil1 detectable nucleoli, arrowheads; Piwil1 undetectable nucleoli, C; control without inhibitors, IC; initial control. (C) Immunostaining of Setdb1 and fibrillarin in wildtype and *meioc*$^{mo/mo}$ spermatogonia. Arrowheads; nucleoli. (D) Co-IP of Piwil1 and Setdb1 using *meioc*$^{mo/mo}$ testes lysate. Piwil1 was detected in Setdb1 IP. (E) Intensities of Setdb1 in nucleoli in wildtype and *meioc*$^{mo/mo}$ spermatogonia. (F, G) ChIP-qPCR analysis of H3K9me3 (F) and Piwil1 (G) levels in 45S-rDNA region in wildtype, *piwil1*$^{+/-}$, and *meioc*$^{mo/mo}$ testes. Position of primers were indicated in Supplemental Figure S3. Mean ± s.d. are indicated. (H) Immunostaining of HP1α and Piwil1 in wildtype and *meioc*$^{mo/mo}$ spermatogonia. Arrowheads; nucleolus. (I) Co-IP of Piwil1 and HP1α using *meioc*$^{mo/mo}$ testis lysate. HP1α was detected in Piwil1 IP. (J) Intensities of HP1α in nucleoli in wildtype and *meioc*$^{mo/mo}$ spermatogonia. *$p < 0.05$, **$p < 0.01$. Scale bars: 10 μm.

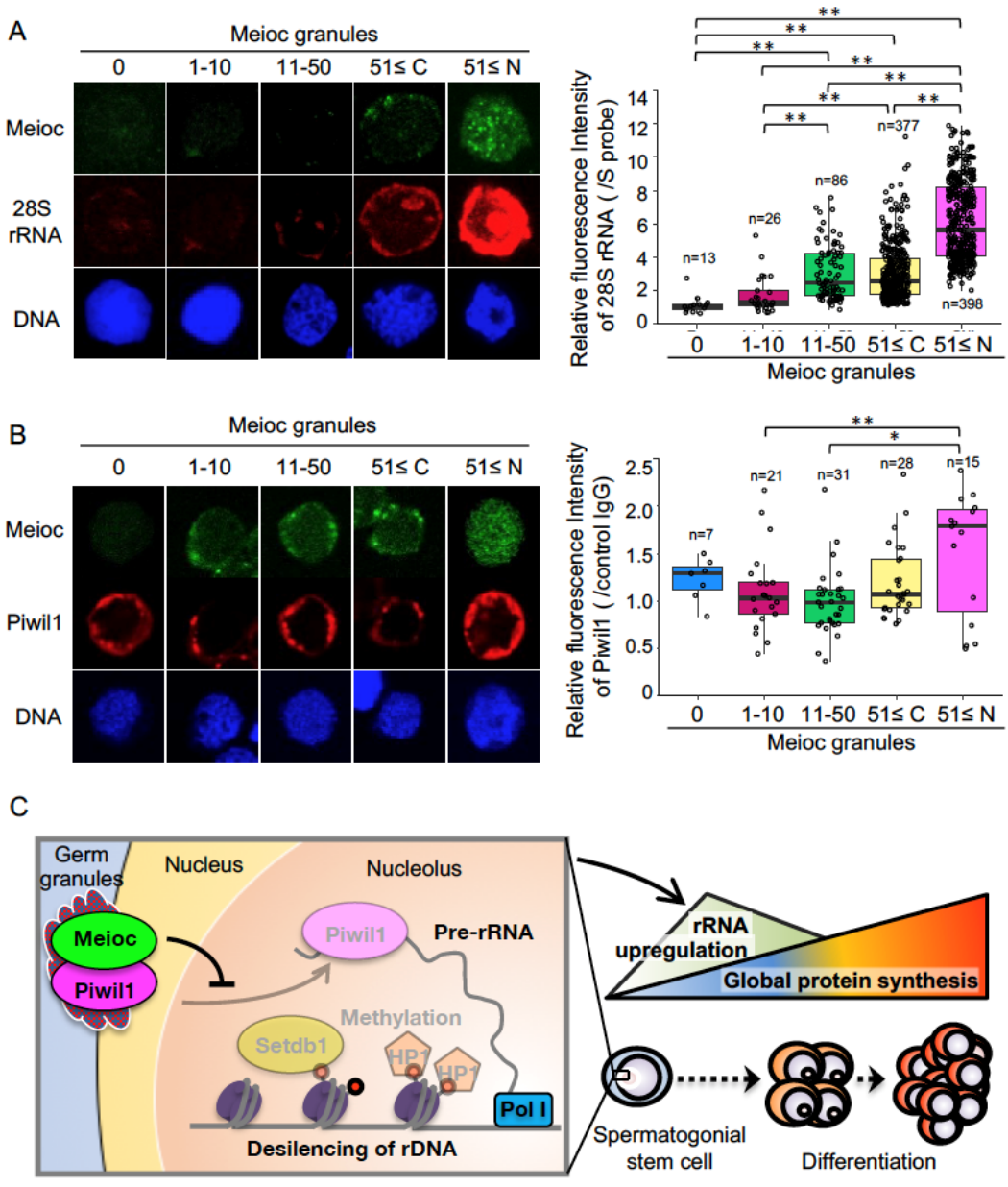

Figure 7. Meioc was required for upregulation of 28S rRNA

(A, B) Expression patterns of 28 rRNA (A) and Piwil1 (B) in isolated *sox17::egfp* spermatogonia, based on the amount of Meioc granules and the localization. Right panels are intensities of 28 rRNA (A) and Piwil1 (B) for each class of the purified wildtype 1-2-cell spermatogonia. 51≤ C and N; 51≤ cytoplasmic and nuclear Meioc granules, respectively. *p <

0.05, **p < 0.01, n: number of analyzed spermatogonia. Scale bars: 10 μm. (C) Graphical abstract. Meioc prevents the nucleolar localization of Piwil1 and its associated Setdb1 and HP1α to upregulate rRNA transcripts that are required for zebrafish SSCs to differentiate.